Composite Structures 270 (2021) 114056

Contents lists available at ScienceDirect

Composite Structures

journal homepage: www.elsevier.com/locate/compstruct

Investigation of energy harvesting in composite beams with different lamination angles under dynamic effects

Fevzi Cakmak Bolat [a,*], Sinan Basaran [b], Murat Kara [a]

[a] Department of Mechanical Engineering, Bolu Abant İzzet Baysal University, Bolu 14280, Turkey
[b] Department of Mechanical Engineering, Bilecik Seyh Edebali University, Bilecik 11230, Turkey

ARTICLE INFO

Keywords:
Composite beam
Flow-induced energy harvesting
Electromagnetic force-induced energy harvesting
Galloping based vibration

ABSTRACT

In this study, energy harvesting from cantilever composite beams produced at different lamination angles was experimentally investigated. In this regard, three different eight layered laminated composite beams are considered, i.e., $\{0^\circ, 90^\circ, 0^\circ, 90^\circ\}_s$, $\{-30^\circ, 60^\circ, -30^\circ, 60^\circ\}_s$ and $\{-45^\circ, 45^\circ, -45^\circ, 45^\circ\}_s$. energy harvest performances were analyzed under different external dynamics inputs by bonding piezoelectric material to the surface of composite beams. Firstly, the composite beam harvesting structure was excited by air-flow. In those experiments, three different types of bluff-body geometry elements were attached to the free end for each of the considered composite beams. In order to determine the maximum power output, different resistors are attached to the piezoelectric material. As a second dynamic input, an electromagnetic actuator operating on the Lorentz principle is used. By using this electromagnetic actuator, the structures are excited by harmonic inputs with different frequencies and frequency-voltage responses were obtained. Besides, vibration amplitudes and voltage outputs were analyzed for both excitation types.

1. Introduction

Small-scale sensors which use low-energy level are outputs of new emerging technology. The energy needs of these products can be met by using renewable energy methods such as harvesting methods of smart materials, which is a popular subject in recent years among researchers. Energy harvesting operations can be performed by designing different energy harvesting structures and using the existing environment dynamics [1–5].

There are many different energy harvest designs available in the literature and studies showing the energy output of them due to different dynamic inputs [6–9]. Some of these different dynamic inputs can be listed such as airflow, vibration, and magnetic field effect. These effects are dynamic factors that enable the harvesting structures to be set into motion or oscillation. Sun et al. [10] attached a galloping profile to the free end of the piezoelectric material glued cantilever beam to provide energy harvesting. Then, they experimentally examined the energy harvesting performance over this structure under open channel based water flow. Wang et al. [11] examined both experimentally and theoretically the energy harvesting performance of a beam with variable thickness. In that study, they compared the energy harvesting capacities of the beam having different types of beams in detail. In another study, a special lead-free piezoelectric nanoparticle-dispersed epoxy resin was experimentally produced and the energy harvesting potential under different conditions was determined [12]. At the same time, the output power of this product under impact load and resonance effect were determined within the scope of the study. Dhakar et al. [13] proposed an energy harvesting structure to facilitate low-frequency power output for a structure. In the paper, a piezoelectric bonded beam was attached to another beam produced from polymer at one end. They experimentally tested the energy harvest performance of the proposed structure. In Ref. [14], the energy harvest that can be obtained from underwater ground-based excitation of piezoelectric composite beam structure is experimentally investigated. The energy output performances were examined in detail by immersing the beam in the water at different heights [14]. In another study, the energy harvesting behaviors of different bi-stable composite beam structures under different external loads are presented [15]. In Ref. [16], the piezoelectric beam element connected to the *meta*-surface bluff-body was placed in a wind tunnel. Experimental analyses based on different resistance and frequency magnitudes were performed for energy harvest analysis. Proposed harvesting structure outputs were analyzed using different types *meta*-surface geometry. Lu et. al. [17] designed a new multilayer piezoelectric energy harvester. As a

* Corresponding author.
E-mail address: fevzicakmakbolat@ibu.edu.tr (F. Cakmak Bolat).

https://doi.org/10.1016/j.compstruct.2021.114056
Received 15 February 2021; Revised 24 April 2021; Accepted 3 May 2021
Available online 6 May 2021

result of the study, it has been experimentally and analytically shown that the multi-layer harvesting structure gives better results than the classical single layer harvesting structure with the same rigidity. Masghouni et. al. [18] have produced a new piezoelectric composite beam based on zinc-oxide nanowires. They tested the performance of their harvesting structure under different vibration sources such as a permanent magnet-based shaker and a water bath sonicator. In another study, instead of the classical support beam used in the literature, a beam consisting of piezoelectric particles was produced [19]. In the scope of that study, a series of analyses were carried out using the finite element method in order to estimate the transverse piezoelectric coefficient (d_{31}) that provides the voltage output from piezoelectric materials. It has been shown by the experiments; the produced beam provides energy output under the effect of mechanical vibration. Zhang et al. [20] applied a nonlinear magnetic field-based force to a nonlinear beam element in their studies and carried out analytical energy harvesting on this structure. A structure consisting of the combination of two piezoelectric patches was analyzed in a vacuum environment based on the same criteria [4]. The response speeds of the proposed structure have been tested using different voltage ranges. The energy harvest performance of a soft dielectric composite was analyzed in Ref. [21]. The proposed composite structure was driven by a shaker and the voltage magnitudes are measured corresponding to the different resistance loads, as a result, power output was determined experimentally. In a more recent study, the energy harvesting performance of a composite wing element under dynamic bending responses was investigated. The proposed model using the finite element method has been verified by comparing it with the models in the literature [22].

As it may be inferred from the literature review, there are limited studies on the energy harvest performance of composite structures. Besides, as far as the authors' knowledge, there is no study on the effect of composite lamination angle on energy harvesting performance. In this study, the energy harvest performances for the eight layered, laminated composite beams produced as $\{0^\circ, 90^\circ, 0^\circ, 90^\circ\}_s$, $\{-30^\circ, 60^\circ, -30^\circ, 60^\circ\}_s$ and $\{-45^\circ, 45^\circ, -45^\circ, 45^\circ\}_s$ were investigated. In this regard, two different dynamic excitations are supplied i.e, flow-induced and Lorentz principle shaker loads. In order to supply the first dynamic load, different bluff-body geometries were produced by 3D printer. Then, they were attached to one end of the cantilever composite beams and the beams were exposed to airflow. Both the displacement of the beams and voltage output from the piezoelectric material with the effect of air-flow was measured. In the latter dynamic load, harmonic inputs at different frequencies are given by an electromagnetic actuator operating according to Lorentz's principle to determine the frequency-dependent displacement and voltage outputs.

Table 1
Properties of the composite beams.

Property (Unit)	Value
Thickness (m) × Width (m)	0.002 × 0.05
Length (m)	0.2
Elasticity along with the first reinforcing fibre (GPa)	21.3
Elasticity along with the second reinforcing fibre (GPa)	21.1
Poisson's ratio	0.161
Shear modulus (GPa)	3.003
Density (kgm^{-3})	1771.21

2. Composite beam specifications

In the article, energy harvesting performances of the laminated thin composite beams are determined. In this regard, eight symmetrically layered beams are examined. The beams are selected to have the same physical properties with different orientation angles. For this purpose, a composite plate with the orientation angle as $\{0^\circ, 90^\circ, 0^\circ, 90^\circ\}_s$ is manufactured by the vacuum infusion technique. Then, the beams are extracted from the composite plate by cutting out beams with the angle of 0°, 30° and 45° from the principal axis. Therefore, three beams orientated as $\{0^\circ, 90^\circ, 0^\circ, 90^\circ\}_s$, $\{-30^\circ, 60^\circ, -30^\circ, 60^\circ\}_s$ and $\{-45^\circ, 45^\circ, -45^\circ, 45^\circ\}_s$ evaluated. The physical and mechanical properties of the beams are presented in Table 1.

3. Energy harvesting structures

The schematic drawing of the energy harvesting structure is presented in Fig. 1. Here, it is aimed to harvest energy for two separate load types, i.e., air load and electromagnetic actuator. Although exper-

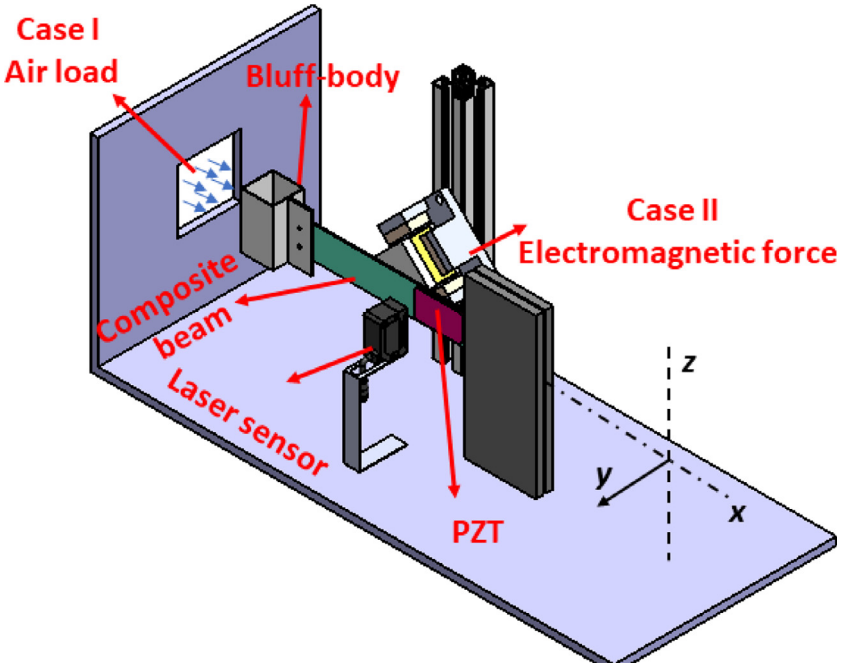

Fig. 1. Energy harvesting structures.

iments are separately conducted for these load types, they are shown in Fig. 1, together. In the first load case (under an air load), galloping geometries with square, triangular and circle geometries are attached to one end of the piezoelectric patch bonded composite beam. Later, under the effect of air-load, the harvesting structure was forced to create a vibration, and energy harvesting was carried out. In the second load case, the piezoelectric patch bonded beam is excited by an electromagnetic actuator at different frequencies to perform energy harvesting.

The piezoelectric material feature is a combination of both the electrical and mechanical behavior of the materials. The equation for the spatial electric displacement is given as $D = \varepsilon E$ with permittivity ε. Combining them for all directions of the material into the so-called coupled equations,

$$\begin{aligned} S &= C_E T + d^T E \\ D &= dT + \varepsilon_T E \end{aligned} \tag{1}$$

where S is the strain vector, T is the stress vector, E is the electric field vector and D is the electric displacement vector. The energy harvesting obtained from the piezoelectric material depends on the material properties and the amount of stress and displacement change that will occur from mechanical energy. The general equation of motion related to displacement for piezoelectric energy generation can be written as follows for this energy harvesting structure.

$$\begin{aligned} (m_b + m_g)\ddot{y} + c\dot{y} + ky - \theta V &= F_{exc} \\ C_{pz}\dot{V} + \tfrac{V}{R} + \theta\dot{y} &= 0 \end{aligned} \tag{2}$$

Where $y, \dot{y}, \ddot{y}$ respectively displacement, velocity, and acceleration of the composite beam element, θ is the electromechanical coupling, C_{pz} is the capacitance of the piezoelectric layer, m_b is the mass of the beam, m_g is the mass of the galloping profile (the three types of galloping geometry elements are produced to have equal masses, 26 g, in the study), F_{exc} is the force acting on the galloping profile, k and c are the stiffness and damping coefficients of the beam element, respectively. The experimental power generated by the piezoelectric transduction is written as follows:

$$P_{pt} = VI = \frac{V^2}{R_l} \tag{3}$$

Here, V is the voltage output value, R_l load resistance.

4. Experimental and numerical determination of stiffness of the composite beams

The energy harvesting event is directly related to the stiffness of the structural element to which the piezoelectric element is attached. Here, the stiffness coefficients of composite beams were determined by using a commercial finite element program and experimentally.

4.1. Numerical determination of stiffness

The beams considered in the paper have equal masses. Therefore, the natural frequencies of the cantilever composite beams may be used to compare the stiffness of the composite beams. In this regard, numer-

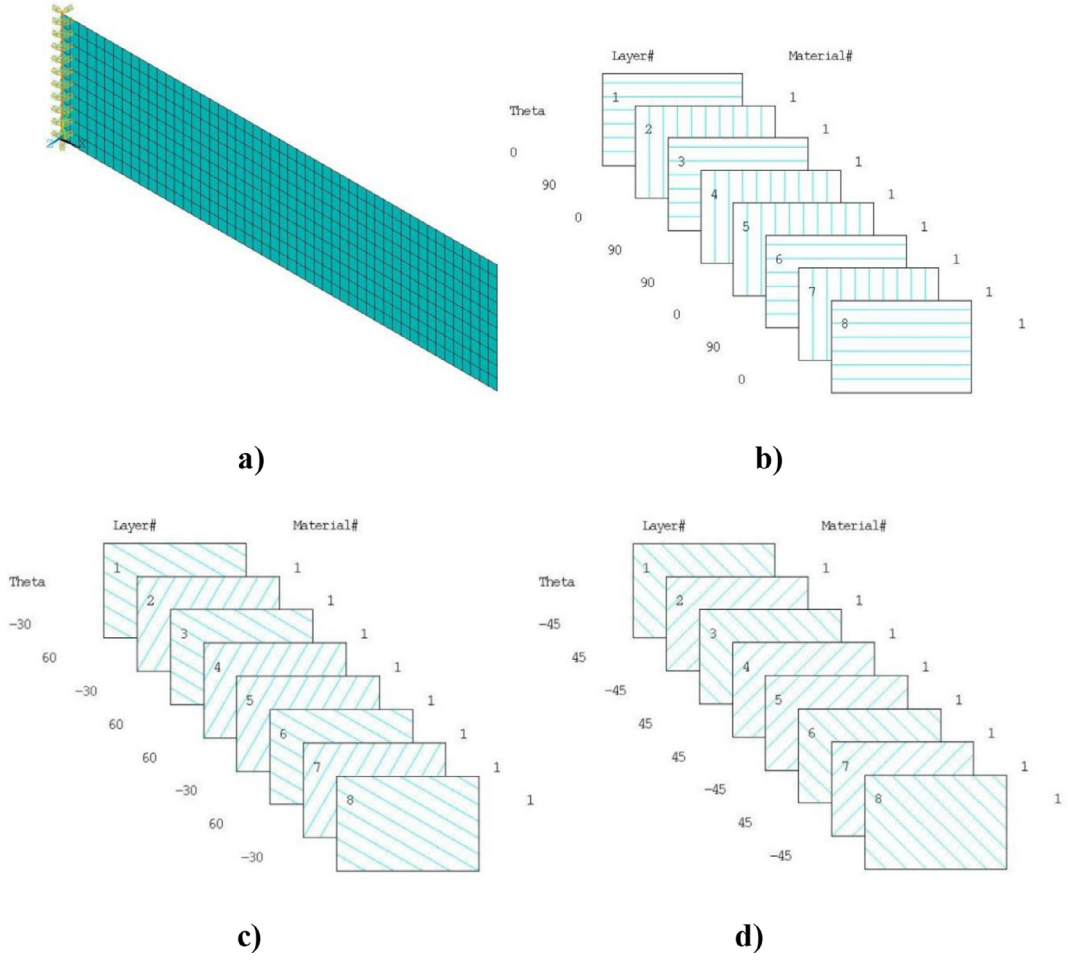

Fig. 2. A numerical model of the composite beams a) the cantilever beam, b) angular orientation of the first beam, c) angular orientation of the second beam, d) angular orientation of the third beam.

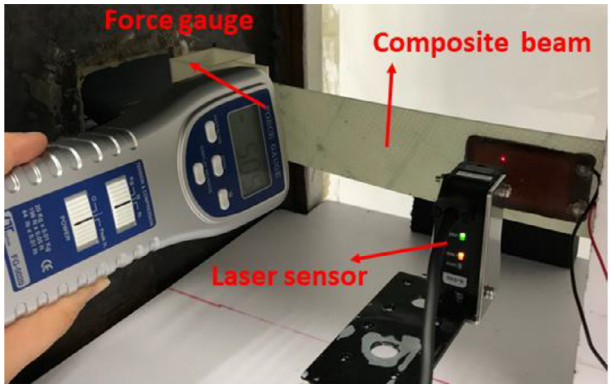

Fig. 3. Stiffness measurement experimental system.

Table 2
Experimental stiffness value.

	$\{0^\circ, 90^\circ, 0^\circ, 90^\circ\}_s$	$\{-30^\circ, 60^\circ, -30^\circ, 60^\circ\}_s$	$\{-45^\circ, 45^\circ, -45^\circ, 45^\circ\}_s$
Experimental stiffness (N/m)	1.5122×10^3	1.303×10^3	1.152×10^3

ical models of the beams are constructed as thin plates with an aspect ratio of $l_x/l_y = 4$ via the finite element method. In finite element computations, Shell181 element of ANSYS APDL is utilized for the composite beam which uses the first-order shear deformation theory and is suitable for analyzing thin or moderately thick laminated shells. It has six degrees of freedom (DOF) at each node, i.e., three translational and three rotational DOFs. Eight layered beams are constructed according to their properties and angular orientation by using ANSYS as shown in Fig. 2a. In Fig. 2b–d, the angular orientations of the beams are presented. The structures are meshed by 10x50 elements and natural frequencies are computed.

The numerical natural frequencies are determined as 25.5 Hz, 19.8 Hz and 18.6 Hz for the beams having the orientation angle of $\{0^\circ, 90^\circ, 0^\circ, 90^\circ\}_s$, $\{-30^\circ, 60^\circ, -30^\circ, 60^\circ\}_s$ and $\{-45^\circ, 45^\circ, -45^\circ, 45^\circ\}_s$, respectively. The masses of the bluff bodies are 0.026 kg for the three types of geometry. Natural frequencies with the addition of bluff-body geometries as tip mass at the end of the beam, 13.66 Hz, 10.50 Hz and 9.87 Hz for the beams having the orientation angle of $\{0^\circ, 90^\circ, 0^\circ, 90^\circ\}_s$, $\{-30^\circ, 60^\circ, -30^\circ, 60^\circ\}_s$ and $\{-45^\circ, 45^\circ, -45^\circ, 45^\circ\}_s$, respectively. Since the beams have equal masses, the relation between the stiffness (K) of the beams may be written as $K_{0,90} > K_{-30,60} > K_{-45,45}$ where the sub-index indicates the orientation of beams.

4.2. Experimental determination of stiffness

Fig. 3 shows an experimental test setup to determine the stiffness of composite beams. Stiffness was measured by recording the displacement values (measured by laser sensor) generated by the force gauge for 3 different types of composite beams used in the experiment. Calculated stiffness' were tabulated in Table 2.

As the second verification experiment, free vibration responses on the time-domain were measured. In this regard, the beams are released from the same reference setpoint and time-domain results are obtained as shown in Fig. 4. Having higher displacement amplitudes indicate the beams having lower stiffness.

It may be inferred from Fig. 4 that, the results of free vibration displacement of the beams are compatible with the stiffness values obtained by force gauge measurements and numerical results.

5. Experimental system and results

As stated earlier, the energy harvesting performance of composite beams are examined under two different dynamic load cases, i.e., air flow-based and electromagnetic based excitations. Experimental systems corresponding to these excitation cases are presented in Fig. 5a,b. PI's 876-A.12 type piezoelectric material has adhered to the composite beams. The displacement information was measured by the Keyence IL30 laser sensor and processed on the Dspace 1104 data acquisition card. An oscilloscope is used to measure the voltage outputs. For the electromagnetic excitation, a Lorentz actuator was produced as shown in Fig. 5b to provide different frequency inputs. This actuator was controlled by Pololu 18v15 current driver and measurements were taken by providing input at different frequencies.

In Fig. 5a, three different types of galloping geometry namely square, triangle, and circle were considered to the composite beam end for the experiments performed under air load. The effects of these different galloping geometries on energy harvest under air load have been studied. In Figs. 6–8, the voltage and displacement results of different types of galloping geometries under air load are given.

As it may be observed from Figs. 6–8, the higher displacement and voltage amplitudes are evaluated for the beams having lower stiffness

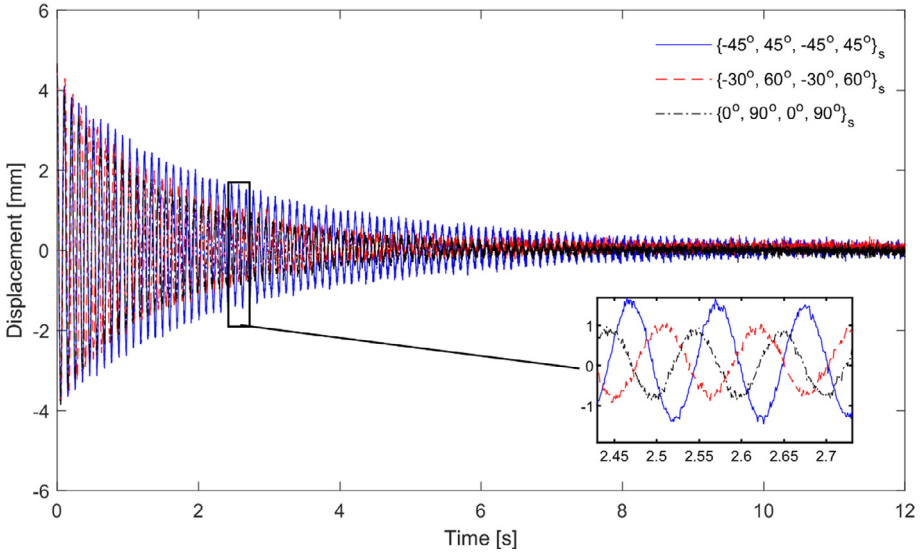

Fig. 4. Experimental free vibration results.

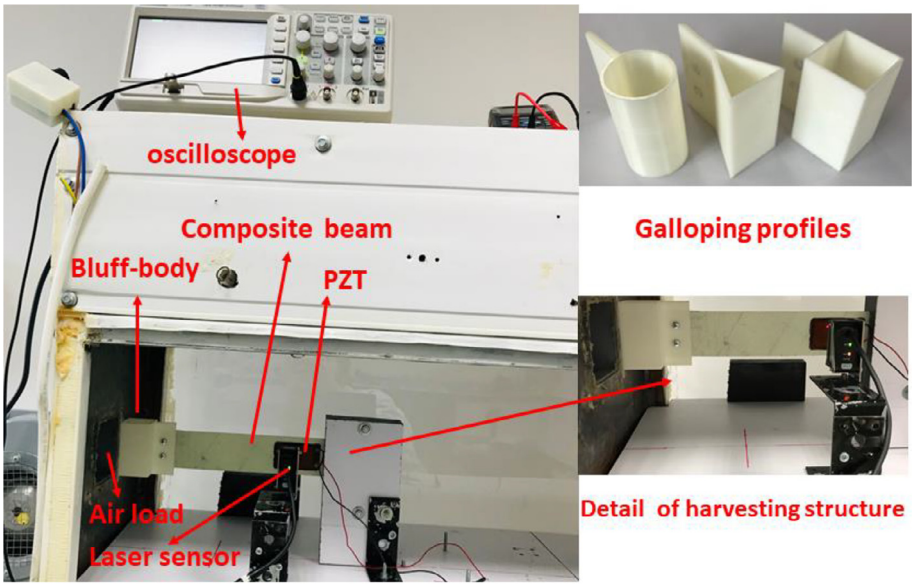

(a)

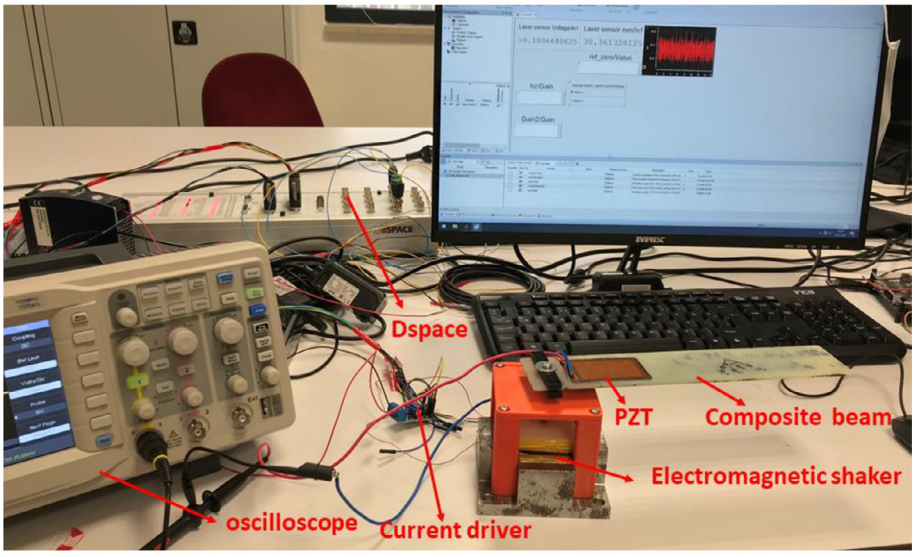

(b)

Fig. 5. Experimental system a) air load-based b) electromagnetic shaker-based.

as expected. On the contrary, voltage amount has a direct proportion with the stiffness of the beams. Besides, rectangle and triangle galloping profiles induce much higher vibration amplitudes with respect to circular profiles for all composite beams. In Fig. 9, measured voltage outputs for the rectangle galloping profile for all composite beams are compared.

As another experimental study, optimal resistor load is determined in order to obtain maximum power output from the considered composite structures under air load for all galloping structures. In this regard, a set of resistor loads are utilized i.e., 1 MΩ, 330 kΩ, 68 kΩ, and 6.8 kΩ. The power outputs obtained under these resistor loads are given in Figs. 10–12 for the square, triangle, and circle profiles, respectively.

As seen in Fig. 10, the maximum power output for square galloping geometry was obtained from a composite beam with a fibre orientation of $\{-45^\circ, 45^\circ, -45^\circ, 45^\circ\}_s$ as 8.3 mW. Then, 5.9 mW from $\{-30^\circ, 60^\circ, -30^\circ, 60^\circ\}_s$ composite beam and 4.3 mW from $\{0^\circ, 90^\circ, 0^\circ, 90^\circ\}_s$ composite beam were obtained, respectively. It is obvious that the results obtained are compatible with the stiffness tests.

Fig. 11 states that the maximum power output for triangular galloping geometry was obtained from the composite beam with fibre orientation $\{-45^\circ, 45^\circ, -45^\circ, 45^\circ\}_s$ as 7.9 mW. Besides, 4.3 mW from composite beam with $\{-30^\circ, 60^\circ, -30^\circ, 60^\circ\}_s$ fibre orientation and 3.4 mW from $\{0^\circ, 90^\circ, 0^\circ, 90^\circ\}_s$ composite beam were obtained.

While the circle galloping geometry is connected in Fig. 12, the maximum power output was obtained from a composite beam with $\{-45^\circ, 45^\circ, -45^\circ, 45^\circ\}_s$ fibre orientation as 0.008 mW. Then, from the composite beam with $\{-30^\circ, 60^\circ, -30^\circ, 60^\circ\}_s$ fibre orientation, 0.0077 mW and from the composite beam with $\{0^\circ, 90^\circ, 0^\circ, 90^\circ\}_s$ fibre angles was obtained as 0.0054 mW. Besides, one may state from Figs. 10–12 that, the optimum power output was obtained by using 68 kOhm resistive load for all composite beams.

As the second load system (electromagnetic excitation), energy harvesting performance at different excitation frequencies is investigated.

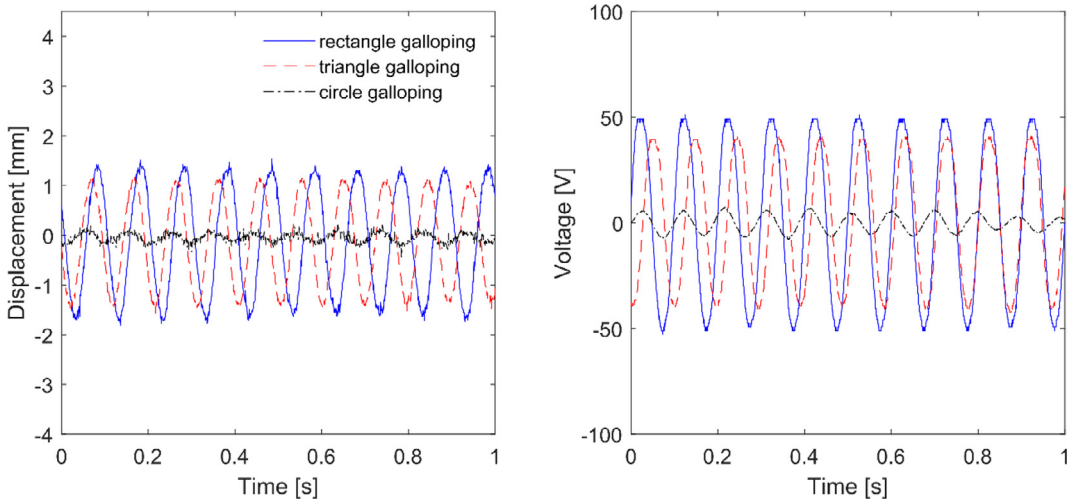

Fig. 6. (a){0°, 90°, 0°, 90°}$_s$ composite beam displacement results. (b) voltage (no-load) results.

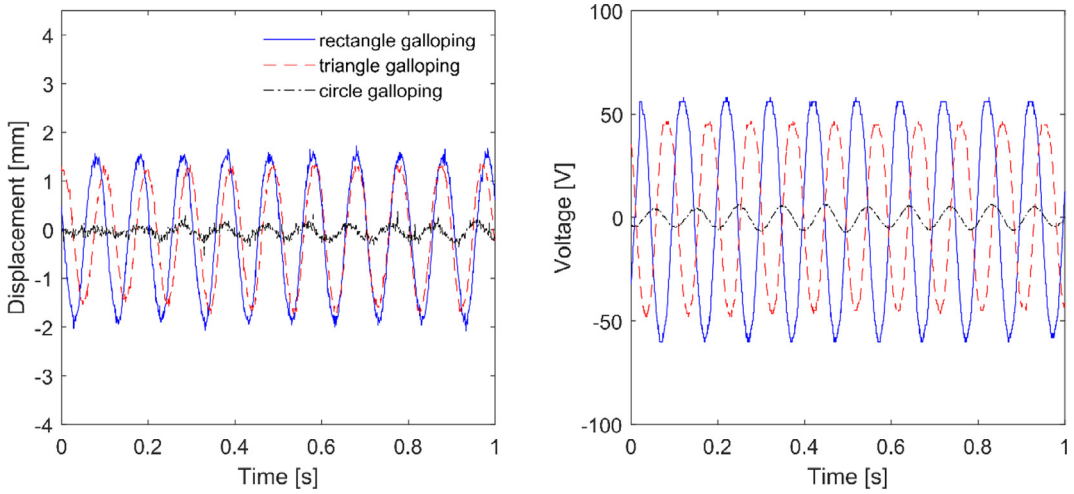

Fig. 7. (a) {−30°, 60°, −30°, 60°}$_s$ composite beam displacement results. (b) voltage (no-load) results.

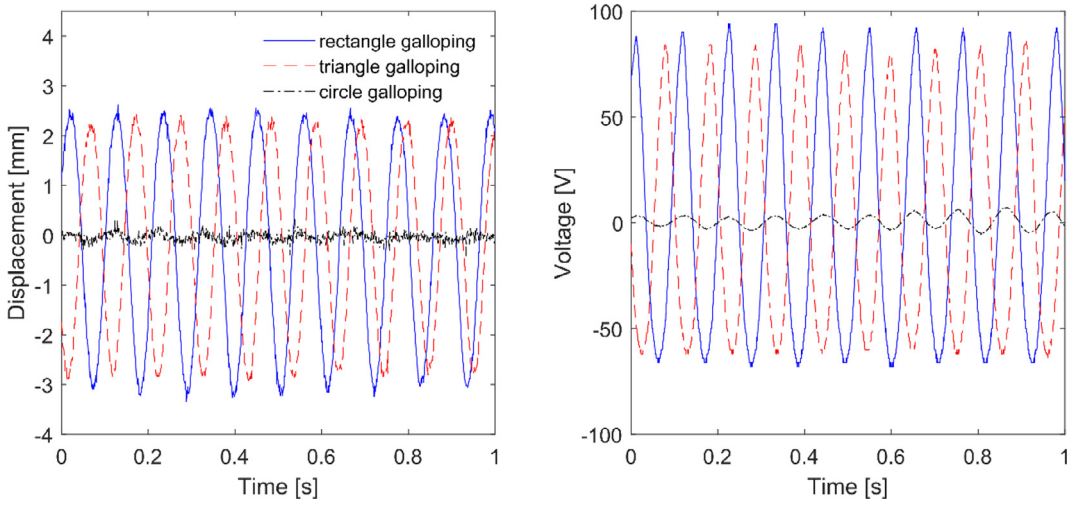

Fig. 8. (a) {−45°, 45°, −45°, 45°}$_s$ composite beam displacement results. (b) voltage (no-load) results.

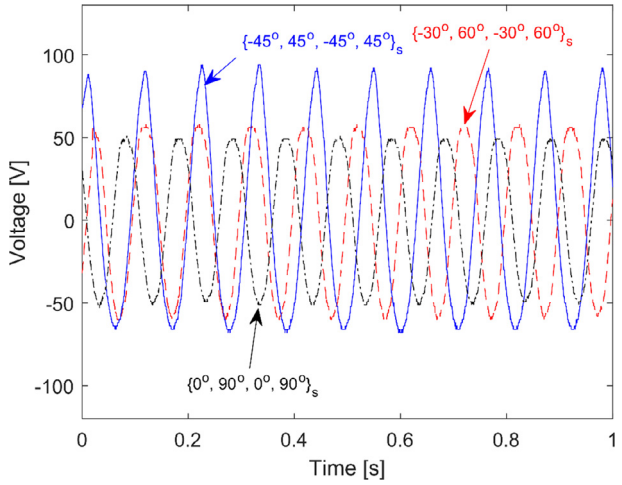

Fig. 9. Comparison of the composite beams voltage output for the rectangular galloping profile.

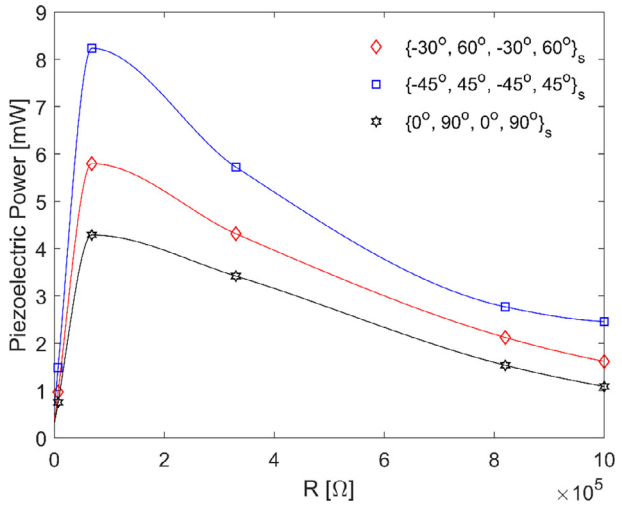

Fig. 10. Rectangle galloping profile experimental power output results.

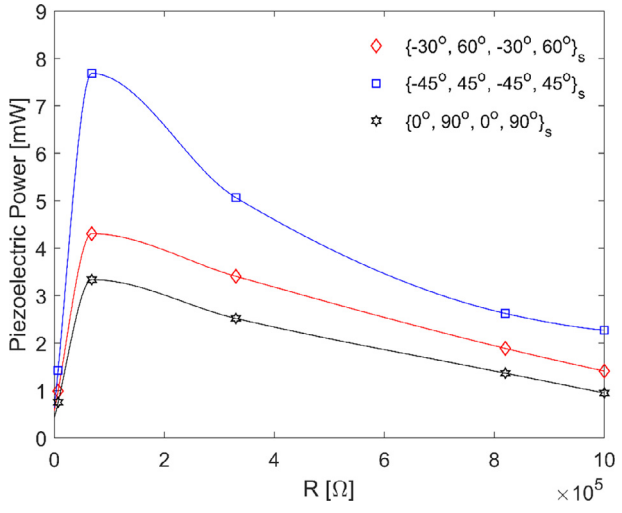

Fig. 11. Triangle galloping profile experimental power output results.

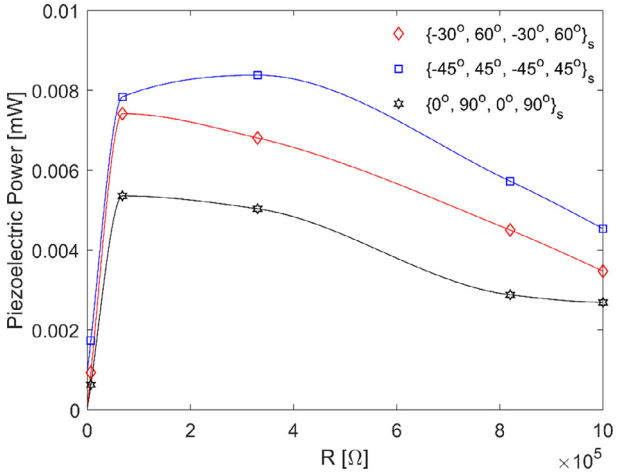

Fig. 12. Circle galloping profile experimental power output results.

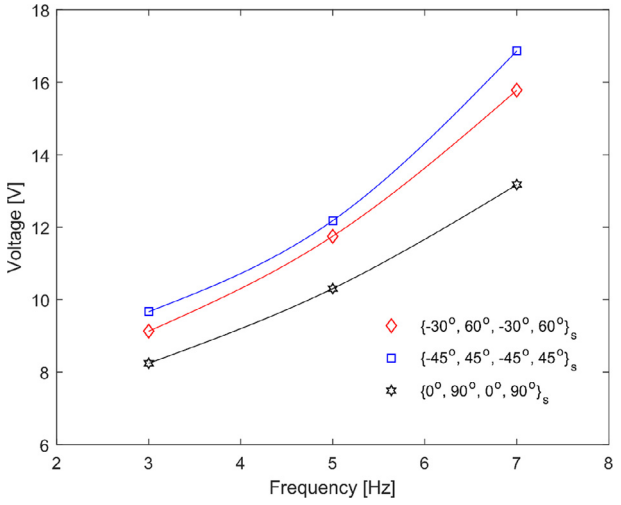

Fig. 13. Comparison of the composite beams voltage output at different excitations frequency.

Experimental voltage outputs of composite beams having {0°, 90°, 0°, 90°}$_s$, {−30°, 60°, −30°, 60°}$_s$, and {−45°, 45°, −45°, 45°}$_s$ fibre orientation are shown in Figure 14. These results are obtained under three different frequencies (i.e., 3 Hz, 5 Hz, and 7 Hz) by utilizing the experimental setup shown in Fig. 5-b. Voltage output amplitudes corresponding to the considered frequencies for the composite beams are compared in Fig. 13.

Fig. 13 states that, as the frequency increases, the voltage values obtained from the beams also increase. Besides, the measured results are also consistent with the ones of the air-flow load condition.

6. Conclusions

In this study, energy harvesting performances of composite beams with {0°, 90°, 0°, 90°}$_s$, {−30°, 60°, −30°, 60°}$_s$ and {−45°, 45°, −45°, 45°}$_s$ fibre angles were analysed. Two different dynamic condition conditions are revealed to obtain energy harvesting from these composite beams. In the first case, these composite beams were connected to an air tunnel and the effects of bluff-body geometries with the different surface areas on the vibrations of the composite beams were revealed. Optimum power output has been obtained by etching resistance loads of different sizes. Maximum power output among the considered beams and bluff-body geometry was obtained for square bluff-

body connected to the beams having $\{-45^{\circ}, 45^{\circ}, -45^{\circ}, 45^{\circ}\}_s$ orientation. Besides, optimum power outputs were obtained from all galloping geometries with the 68 kOhm resistor load. In the second excitation case, an electromagnetic shaker working according to the Lorentz principle is used. The composite beams are excited by this shaker at three different frequencies i.e., 3, 5, and 7 Hz. In these experiments, as the excitation frequency increases, the voltage values obtained from the beams also increase. Besides, these results are consistent with the ones of the results measured under air-flow.

Declaration of Competing Interest

The authors declare that they have no known competing financial interests or personal relationships that could have appeared to influence the work reported in this paper.

References

[1] Bolat FC, Basaran S, Sivrioglu S. Piezoelectric and electromagnetic hybrid energy harvesting with low-frequency vibrations of an aerodynamic profile under the air effect. Mech Syst Sig Process 2019;133():106246.

[2] Erturk A, Inman DJ. Broadband piezoelectric power generation on high-energy orbits of the bistable Duffing oscillator with electromechanical coupling. J Sound Vib 2011;330(10):2339–53.

[3] Bolat FC, Sivrioglu S. Energy harvesting using an aerodynamic blade element at resonant frequency with air excitation. Smart Struct Syst 2019;24(3):379–90.

[4] Tan D, Yavarow P, Erturk A. Nonlinear elastodynamics of piezoelectric macro-fiber composites with interdigitated electrodes for resonant actuation. Compos Struct 2018;187:137–43.

[5] Wang J et al. Dynamics of the double-beam piezo-magneto-elastic nonlinear wind energy harvester exhibiting galloping-based vibration. Nonlinear Dyn 2020. https://doi.org/10.1007/s11071-020-05633-3.

[6] Lai Z et al. A hybrid piezo-dielectric wind energy harvester for high-performance vortex-induced vibration energy harvesting. Mech Syst Signal Process 150 2021;107212. https://doi.org/10.1016/j.ymssp.2020.107212.

[7] Mujtaba A et al. Hydrodynamic energy harvesting analysis of two piezoelectric tandem flags under influence of upstream body's wakes. Appl Energy 2021;282:. https://doi.org/10.1016/j.apenergy.2020.116173116173.

[8] Bolat FC. An experimental analysis and parametric simulation of vibration-based piezo-aeroelastic energy harvesting using an aerodynamic wing profile. Arab J Sci Eng 2020:1–8.

[9] Maamer B et al. A review on design improvements and techniques for mechanical energy harvesting using piezoelectric and electromagnetic schemes. Energy Convers Manage 2019;199:. https://doi.org/10.1016/j.enconman.2019.111973111973.

[10] Sun W, Tan T, Yan Z, Zhao D, Luo X, Huang W. Energy harvesting from water flow in open channel with macro fiber composite. AIP Adv 2018;8(9):095107.

[11] Wang B, Luo X, Liu Y, Yang Z. Thickness-variable composite beams for vibration energy harvesting. Compos Struct 2020;112232.

[12] Wang Z, Kurita H, Nagaoka H, Narita F. Potassium sodium niobate lead-free piezoelectric nanocomposite generators based on carbon-fiber-reinforced polymer electrodes for energy-harvesting structures. Compos Sci Technol 2020;199:108331.

[13] Dhakar L et al. A new energy harvester design for high power output at low frequencies. Sens Actuators, A 2013;199:344–52.

[14] Cha Y, Kim H, Porfiri M. Energy harvesting from underwater base excitation of a piezoelectric composite beam. Smart Mater Struct 2013;22(11):115026.

[15] Dai F, Pan D. Piezoelectric energy harvesting based on bi-stable composite laminate. Energy Harvest 2018:63–82. https://doi.org/10.5772/intechopen.76193.

[16] Wang J, Sun S, Tang L, Hu G, Liang J. On the use of metasurface for Vortex-Induced vibration suppression or energy harvesting. Energy Convers Manage 2021;235:113991.

[17] Lu Q et al. A novel composite multi-layer piezoelectric energy harvester. Compos Struct 2018;201:121–30. https://doi.org/10.1016/j.compstruct.2018.06.024.

[18] Masghouni N et al. Investigating the energy harvesting capabilities of a hybrid ZnO nanowires/carbon fiber polymer composite beam. Nanotechnology 2015;26(9):. https://doi.org/10.1088/0957-4484/26/9/095401095401.

[19] Grzybek D et al. Piezoelectric particulate composite for energy harvesting from mechanical vibration. Materials 2020;13(21):4925. https://doi.org/10.3390/ma13214925.

[20] Zhang X et al. A tri-stable piezoelectric vibration energy harvester for composite shape beam: Nonlinear modeling and analysis. Sensors 2020;20(5):1370. https://doi.org/10.3390/s20051370.

[21] Pruvost M et al. Integration of a soft dielectric composite into a cantilever beam for mechanical energy harvesting, comparison between capacitive and triboelectric transducers. Sci Rep 2020;10(1):1–14. https://doi.org/10.1038/s41598-020-77581-2.

[22] Akbar M, Curiel-Sosa JL. Piezoelectric energy harvester composite under dynamic bending with implementation to aircraft wingbox structure. Compos Struct 2016;153:193–203. https://doi.org/10.1016/j.compstruct.2016.06.010.